Alternative splicing of a TPR domain determines mitochondrial versus plastid function of the only CLU family protein in *Marchantia polymorpha*

Maria Lozano-Quiles[1], Parth K. Raval[1], Sven B. Gould[2]

[1]Institute for Molecular Evolution, Heinrich-Heine-University Düsseldorf, 40225 Düsseldorf, Germany

[2]Institute for Population Genetics, Heinrich-Heine-University Düsseldorf, 40225 Düsseldorf, Germany

Corresponding author: gould@hhu.de

Abstract

In plant cells, the multi-domain proteins FRIENDLY and REC regulate the cellular organization, distribution and proliferation of mitochondria and plastids, respectively. Both proteins share a similar overall domain architecture and belong to the larger CLUSTERED MITOCHONDRIA (CLU) superfamily. Domains of CLU proteins have been shown to interact with translation related proteins, tRNA synthetases and even mRNA, but their exact modes of operation remain cryptic and how organelle specificity of CLU paralogs in plant cells is achieved unknown. We characterized the single CLU family protein of the liverwort *Marchantia polymorpha* that we demonstrate to be transcribed either with or without exon 22, which changes the configuration of the TPR domains in the C-terminus. Knockout of Mp*CLU* affects both mitochondria and plastids, and independent rescues show that the splice variant with exon 22 (MpCLU^{22}) serves mitochondrial- and the one lacking exon 22 (MpCLU^{spl22}) plastid biology. The CLU-C domain of the protein is responsible for nuclear localisation and expressed alone induces a phenotype that differs in photosynthesis performance and transcriptome changes from that of the knockout of Mp*CLU*. Our results identify the C-terminal TPR motif to be responsible for organelle specificity in plants and they provide an example of how genome reformatting and gene loss can be compensated for by the alternative splicing of a single exon.

Keywords: *Marchantia*, Alternative splicing, Chloroplasts, Mitochondria, Organelle distribution, TPR domain

ORCID of MLQ: 0009-0002-5826-7317

ORCID of PKR: 0000-0001-6151-437X

ORCID of SBG: 0000-0002-2038-8474

Introduction

The origin of eukaryotes added a new type of cell to the tree of life, a cell characterized by several membrane-bound compartments that together form the endomembrane system. Eukaryotic compartments evolved during eukaryogenesis in an archaeal host, in an unknown order, and likely as a consequence of endosymbiosis (Raval et al., 2022; Richards et al., 2024). The cytosolic space allocated to and the distribution of any given compartment is no coincidence, but the result of a continuously orchestrated feedback loop (Chan and Marshall, 2010; Lloyd AC, 2013). For example, the nuclear volume is fine-tuned with respect to cell size by proteins of the lamin family, and the LINC and nuclear pore complex (Jevtić et al., 2014; Y. Wu et al., 2022). The Golgi apparatus is more dynamic, its volume being regulated by proteins such as Sec16 and Src kinases and depending on incoming versus outgoing vesicle flux (Sengupta and Linstedt, 2011). For two compartments, mitochondria and plastids, the regulation of their number, volume and distribution is a special case, because both were once free-living bacteria and they hence cannot be synthesised *de novo* from scratch.

One gene associated with intracellular mitochondrial distribution was initially identified in *Dictyostelium* and named *cluA* due to the clustering of mitochondria observed upon its deletion (Zhu et al., 1997). Subsequently characterized orthologues in *Saccharomyces* (*clu1*) (Fields SD et al., 1998), *Drosophila* (*clueless*) (Cox and Spradling, 2009), human (*cluH*) (Gao et al., 2014), and *Arabidopsis* (*friendly mitochondria*, *fmt* or *friendly*) (Logan et al., 2003) established the CLUSTERED MITOCHONDRIA (CLU) superfamily, as defined by the presence of CLU domains. This was followed by the characterisation of a CLU family protein from *Arabidopsis*, which was found to influence plastid number and morphology, and termed REDUCED CHLOROPLAST COVERAGE (REC) (Larkin et al., 2016). Orthologues thereof have since been analysed in the monkeyflower *Erythranthe lewisii* (termed REDUCED CAROTENOID PIGMENTATION or RCP) (Stanley et al., 2020), in tomato (SlREC) and other plants (Hu et al., 2024), and it was suggested that these plastid regulators once originated after the gene duplication of a mitochondrion-associated CLU protein (Hu et al., 2024; Stanley et al., 2020).

Indeed, plastid-type CLU proteins (CLU^{pl}) are remarkably similar to CLU proteins associated with mitochondrial biology (CLU^{mt}). With few exceptions, they share the same identifiable domains, including multiple eponymous CLU domains and a series of tetratricopeptide repeats (TPR) in the C-terminus of the protein (Fig. 1a). This raises the question of how CLU paralogues within the same species (e.g. FRIENDLY vs REC in *Arabidopsis*) serve each organelle specifically and how the CLU^{pl} subfamily functionally diverged from the CLU superfamily. Despite the high level of sequence and domain architecture similarities, CLU^{mt} and CLU^{pl} proteins show distinct subcellular localisation and functions. CLU^{mt} protein localisation is predominantly cytosolic, but sometimes they are found to cluster around mitochondria (Cox and Spradling, 2009; El Zawily et al., 2014; Kumar et al., 2002) and to contribute to mitochondrial distribution, fission, and mitophagy (Ayabe et al., 2021; Cox and Spradling, 2009; El Zawily et al., 2014; Fields SD et al., 1998; Gao et al., 2014; Zhu et al., 1997). They interact with ribosomal and other translational proteins and have been reported to assist with the import of nuclear-encoded mitochondrial proteins (Gao et al., 2014; Ma et al., 2021; Sen and Cox, 2016; Yang et al., 2022). In contrast, select CLU^{pl} proteins (e.g. At*REC1* and its homologues) show cyto-nuclear localisation and they regulate the number and cellular space allocated to plastids (Larkin et al., 2016), as well as chlorophyll- and carotenoid- biosynthesis (Hu et al., 2024; Stanley et al., 2020). The molecular details of how the CLU^{mt} and CLU^{pl} subfamilies distinguish between the two organelles, how they shift localisation from the cytosol to the nucleus or how they secure organelle homeostasis, however, remains uncertain.

Ancestral state reconstruction of the CLU superfamily has revealed a curious distribution of homologs among bryophytes (liverworts, hornworts and mosses) (Raval et al., 2024), a group reported to encode a larger repertoire of gene families than vascular plants (Dong et al., 2025). The moss

Physcomitrium patens encodes the canonical set of CLU paralogues for both organelles, but the hornwort *Anthoceros agrestis* only two CLU^{pl} proteins, and the liverwort *Marchantia polymorpha* only a single CLU^{mt} protein. In this study, we characterized the single CLU superfamily member of *M. polymorpha* (Mp6g08800). Our data uncover (i) how the CLU^{pl} and CLU^{mt} subfamilies diverged during the time of plant terrestrialization, (ii) the domain being imported by the nucleus, and (iii) how the alternative splicing of a single Mp*CLU* gene leads to two proteoforms with distinct functional fates. The latter presents us with a unique feature from which to better understand this protein family and the overall mechanism of differential organelle volume and dispersion regulation that is so far lacking from the existing literature on both animals and plants.

Results

The CLU^{mt} superfamily originated during eukaryogenesis and the CLU^{pl} subfamily in the algal ancestors of land plants

A range of different proteins contribute to cellular space allocation and volume regulation of mitochondria and plastids, the two organelles of endosymbiotic origin (Larkin, 2022; Logan et al., 2003). Comparative genomics show that most of the plastid regulators originated in streptophyte algae and duplicated subsequently in land plants (Fig. S1), in line with the general trend of an increasing number of organelle-associated proteins in land plants (Raval et al., 2024). A global screening of InterProScan (Fig. S2) shows that the eponymous clu domain is absent from prokaryotic genomes, but conserved across all eukaryotic supergroups. Clustering of 614 CLU proteins of 133 eukaryotes clearly separated CLU superfamily into CLU^{mt} and CLU^{pl} subfamilies (Fig. S3). The CLU^{pl} proteins are absent in glauco-, rhodo- and chlorophyte algae, tracing their previously suggested origins from CLU^{mt} (Hu et al., 2024) to streptophyte algae. Subsequent divergence of the two organelle-specific subfamilies is evident in predicted domain architectures (Fig. 1). The GSKIP domain, likely connected to mitochondrial metabolism and morphology (Chou et al., 2006; Loh et al., 2015; N. S. Wu et al., 2022), is gradually disappearing from the CLU^{pl} homologs (Fig. 1b). Arrangement of the TPR domains also diverged between CLU^{mt} and CLU^{pl} proteins, as well as between the CLU^{mt} proteins of plants versus animals (Fig. 1a, Fig. S4). The region following the TPR motif has been extended by approximately 500 amino acids on average in the CLU^{pl} proteins (Fig. 1c).

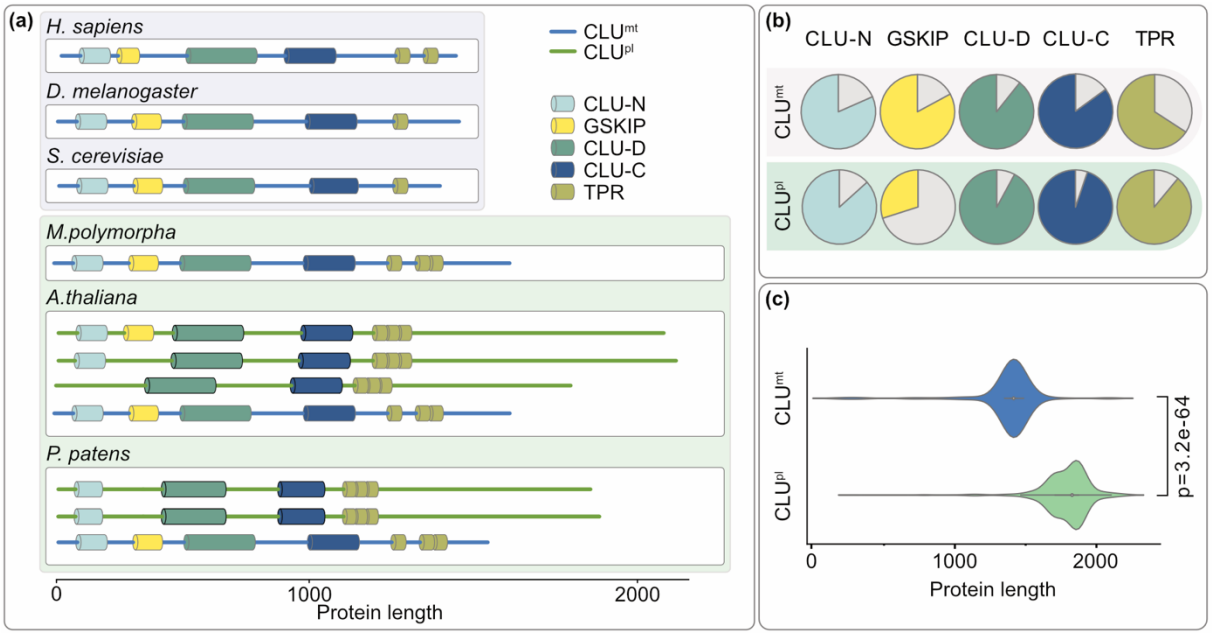

Fig. 1: CLU^{mt} and CLU^{pl} subfamilies differ in their domain architecture and length. (a) Functional domain architectures based on InterPro scans for exemplary animal and plant CLU proteins. **(b)** A summary for 154 plastid- and 460 mitochondria-type CLU proteins from 133 eukaryotes with respect to the presence (coloured portion of the pie chart) or absence (light grey) of a given motif. **(c)** Lengths (in amino acids) of CLU homologues (p-values calculated using Wilcoxon Mann Whitney rank-sum test).

Marchantia encodes a single *clu* gene that is alternatively spliced at exon 22

For the single *Marchantia CLU* gene (Mp6g08800), which clusters with the CLU^{mt} proteins (Fig. S3a), two gene models are annotated. They differ at exon 22, leading either to a splice variant with (MpCLU^{22}) or without exon 22 (MpCLU^{spl22}). The alternative splicing generates two proteoforms that differ in a stretch of only 23 amino acids immediately upstream of the TPR motif (Fig. 2a). This additional exon is enriched in proline residues, through which is it is likely to bend the peptide chains, particularly affecting the alpha-helix rich TPR motifs. As per this expectation, MpCLU^{22} and MpCLU^{spl22} are predicted to differ in the TPR motif encoding region (Fig. 2b), which also matches our results on the sequence divergence that helps to specifically allocate a CLU protein to either the mitochondrial or plastid subfamily (Fig. 1; Fig. S4a). Furthermore, the acetylation of two lysines in At*FMT* appears to be linked with its mitochondrial specificity (El Zawily et al., 2014) and splicing leads to the loss of a lysine residues in Mp*CLU* in that very region (Fig. 2a).

To confirm the annotated gene models at the transcript level, we amplified the splicing region of interest from complementary DNA with primer pairs that amplify either one or the other splicing variant (Fig. 2a). The size differences of the products and their sequencing confirmed the expression of both Mp*CLU*^{22} and MpCLU^{spl22} (Fig. 2c). Quantitative PCRs showed that MpCLU^{spl22} is the predominant expression variant (Fig. 2d). The validation of alternative splicing, its predicted impact on a key TPR motif, and the lack of a canonical CLU^{pl} protein led us to hypothesize that alternative splicing of Mp*CLU* evolved to reinstate a CLU^{pl} protein after its loss in *Marchantia*.

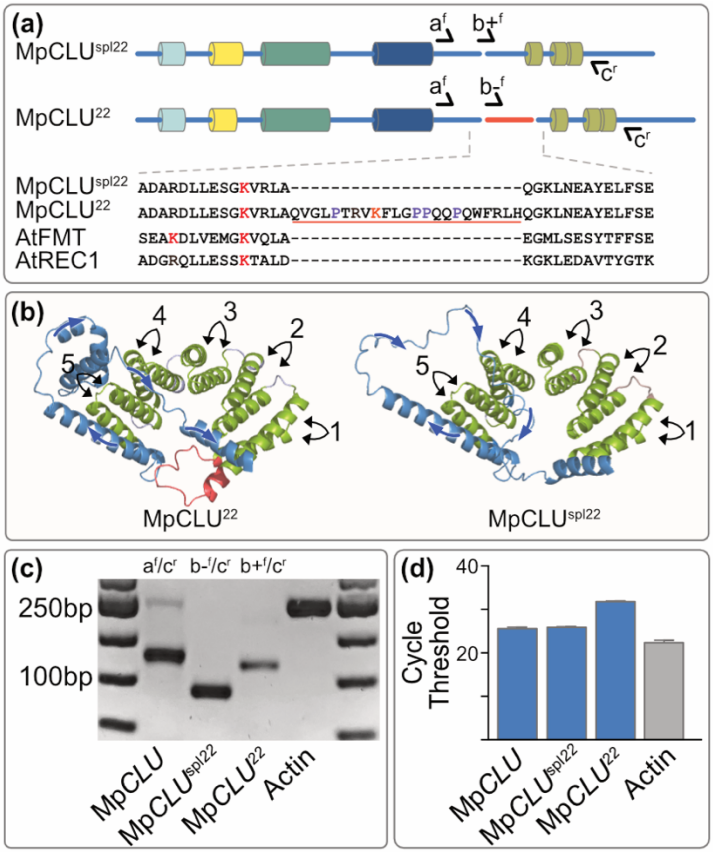

Fig. 2: Mp*CLU* is alternatively spliced at exon 22. (a) Scheme of Mp*CLU* indicating the primer binding sites for specifically amplifying either Mp*CLU*^{22} or Mp*CLU*^{spl22}. Exon22 in red (not at scale). Two lysine residues known to be acetylated in AtFMT and potentially corresponding residues of MpCLU are highlighted in red; proline residues present of exon 22 shown in violet. **(b)** Structural predictions of the TPR region of the two *Marchantia* CLU proteoforms shows that the peptide encoded by exon 22 (in red) affects the angle of an alpha helix (blue arrows) immediately after the fifth TPR domain that returns to the TPR motif. Absence of exon 22 creates a larger gap between the TPR domains. **(c)** PCRs based on complementary DNA (cDNA), indicating the primer sets used on top of each lane. **(d)** Quantitative PCR on the same cDNA as in b.

The CLU-C domain of Mp*CLU* localises to the nucleus and alters growth but not photosynthesis performance

Both mitochondria- and plastid-type CLU family members are multidomain proteins (Fig. 1a). CLU^{mt} proteins have been localised to the cytosol in animals and plants and found to sometimes cluster on the mitochondrial surface (Cox and Spradling, 2009; El Zawily et al., 2014; Kumar et al., 2002), while CLU^{pl} homologs have been reported to localize to the cytosol and the nucleus in several plants (Larkin et al., 2016; Stanley et al., 2020; Zhang et al., 2023). In the liverwort, the full length $MpCLU^{22}$ was found to form small clusters in close proximity to the mitochondrial surface, whereas $MpCLU^{spl22}$ was evenly distributed in the cytosol (Fig. 3a, S5). The CLU-N domain and the CLU-N domain in conjunction with the subsequent GSKIP domain localised to the cytosol, as did the CLU-D domain. In contrast, the CLU-C domain localised to both the nucleus and the chloroplast periphery. This construct's expression furthermore induced a growth phenotype not observed for any of the other constructs (Fig. 3c, S6). CLU-C::Citrine lines grew dwarfed, with a darker and disturbed thallus that formed less gemmae cups (Fig. 3c,d, Fig. 5). Thallus area and biomass were reduced by more than 80% (Fig. 3d) and the plastids appeared elongated and localised to more to the cell's periphery (Fig. 3b).

The darker shade of CLU-C::Citrine lines is likely explained by the increased chlorophyll content of 50% compared to WT, along with elevated lutein, neoxanthin, violaxanthin, and beta-carotene levels (Fig. S7). Despite the doubling of the chlorophyll concentration, no significant changes were measured in photosynthetic efficiency for the CLU-C::Citrine lines, except for a better recovery of Y(II) and ETR after saturation of PSII (Fig. S7). CLU-C::Citrine plants downregulated 240 genes mostly pertaining to cell wall defence and cell surface remodelling, Cu/Ca homeostasis, defence signalling related to salicylic acid, anti-desiccation, and *early light inducible* proteins (ELIPs) (Fig. S14). The C-terminal region including the TPR domain of $MpCLU^{spl22}$ accumulated close to the plastids (Fig. 3b). Multiple attempts at trying to localise the C-terminal region including the TPR domain of $MpCLU^{22}$ failed to generate any viable lines.

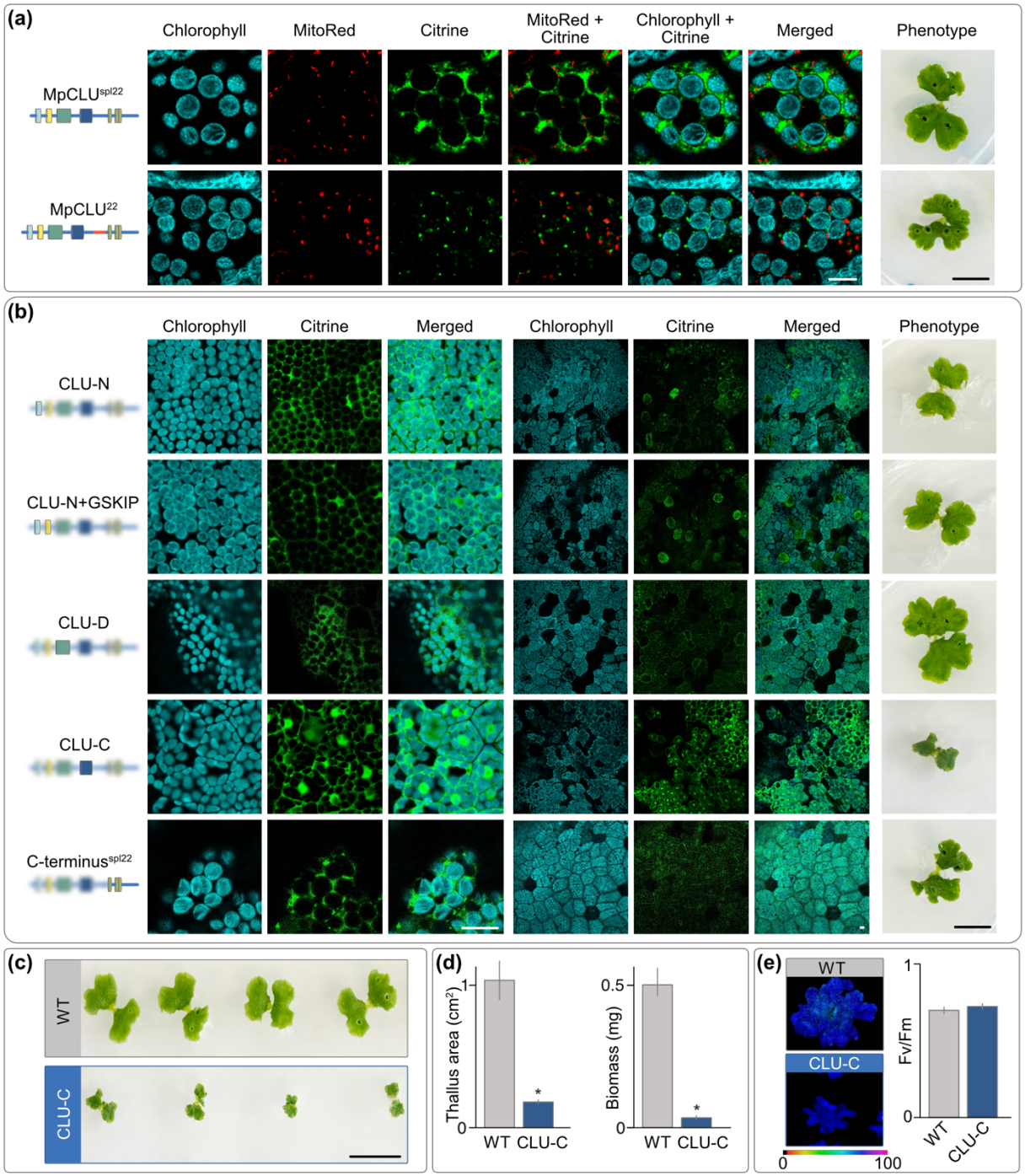

Fig. 3: Subcellular localization of MpCLU and its individual domains. (a) Confocal laser scanning images of MpCLU^{22}::Citrine and MpCLU^{spl22}::Citrine, under 35S promoter in one day-old thalli (plastids imaged through their autofluorescence and mitochondria through MitoTracker Red) and representative images of 14d-old plants harbouring the respective construct. Scale bars from left to right: 10µm and 1cm. **(b)** MpCLU domains fused to Citrine, under 35S promoter in one day old thalli and representative images of 14d-old plants expressing CLU-N::Citrine, CLU-N-terminal::Citrine, CLU-D::Citrine, CLU-C::Citrine and C-terminus^{spl22}::Citrine. Scale bars: 10µm in microscopy pictures and 1cm in phenotyping pictures. **(c)** Representative images of 14d-old WT and CLU-C::Citrine lines. **(d)** Thallus area and biomass measurement of 14d-old WT and CLU-C::Citrine plants, n=10. **(e)** F_v/F_m quantification of WT and CLU-C::Citrine via an Imaging-PAM; n=5. Asterisks indicate significative difference compared to the wild-type (p-value>0.05).

Loss of Mp*CLU* affects both mitochondria and plastids

Using an optimized CRISPR-Cas9 protocol(Sugano et al., 2018), we generated loss of function mutants for Mp*CLU* (Δ*clu*). For a detailed characterisation, we choose a mutant line in which a set of guide RNA introduced an early stop codon (Fig. S8). The Δ*clu* mutants were paler and, in comparison to WT plants, grew at approximately half the rate (Fig. 4a,b). The thallus size and biomass were reduced by approximately 90% (Fig. 4b) and even after six weeks, the formation of gemma cups or gametangia was rarely observed (Fig. 5). At the cellular level, the loss of Mp*CLU* on the one hand resulted in the clustering of mitochondria (Fig. 4c,e, S9) and on the other in 40% fewer plastids. The latter appeared to be compensated for by a 20% increase in organelle size (Fig. 4c,d, S10) and hence the total volume occupied by plastids in Δ*clu* cells is similar to that of WT cells (Fig. S10). Δ*clu* plants downregulated 300 genes involved in cell wall remodelling, abscisic acid biosynthesis and signalling, detoxification, anti-desiccation response, solute/water transport, protein degradation and carbon metabolism, and ELIPs (Fig. S14).

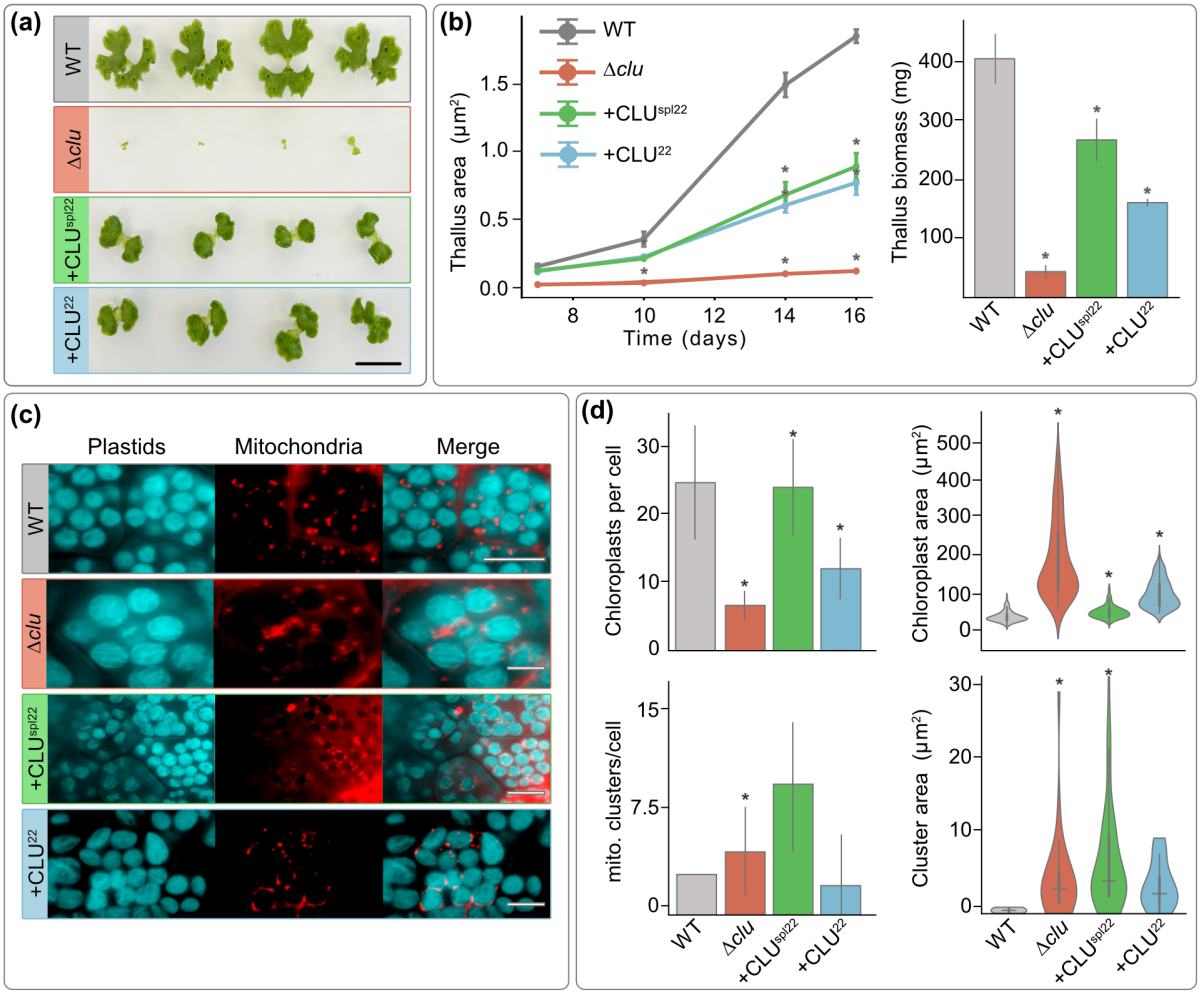

Fig. 4: The difference in the C-terminal TPR domain is responsible for plastid versus mitochondrial phenotype rescue. (a) Representative images of 14d-old WT, Δ*clu*, Δ*clu* + CLU^{spl22} and Δ*clu* + CLU^{22}. Scale bar: 1 cm. **(b)** Area measurement (left) and biomass (right) of the same plants as in a). **(c)** One-day-old gemmae pictures in which mitochondria were stained with Mito-Red. Chloroplasts are monitored through their chlorophyll autofluorescence. Scale bar: 10 µm. **(d)** Above, number of chloroplasts per cell and chloroplast area of WT, Δ*clu* and Δ*clu* rescued with either CLU^{spl22} or CLU^{22}. Below, mitochondrial cluster numbers per cell and the area occupied by mitochondrial clusters of the same plants. Asterisks indicate significative difference compared to the WT (p-value>0.05); n=15 cells per line.

We complemented Δ*clu* by a transfection with either the MpCLU^{22} or the MpCLU^{spl22} splice variants in order to evaluate the effect of the presence and absence of exon 22. The presence of MpCLU^{spl22} in the Δ*clu* background significantly improved the growth rate of the plants, reaching about 70% of the WT thallus area and biomass after 14 days of growth (Fig. 4a, b). While the mitochondria continued to cluster and remain more numerous in number than in WT plants (Fig. 4c, e, S9), the plastid phenotype was fully restored (Fig. 4c, d, S10). The complementation of Δ*clu* with MpCLU^{22} rescued the growth rate in a similar manner as MpCLU^{spl22}: after 14 days, the rescue lines reached about 65% of the WT thallus size and 40% of its biomass (Fig. 4a, b). Yet, while the mitochondria showed a WT-like distribution and no obvious clustering (Fig. 4c, e; S9), the number of chloroplasts and their combined volume occupied remained similar to that Δ*clu* (Fig. 4c, d, S10).

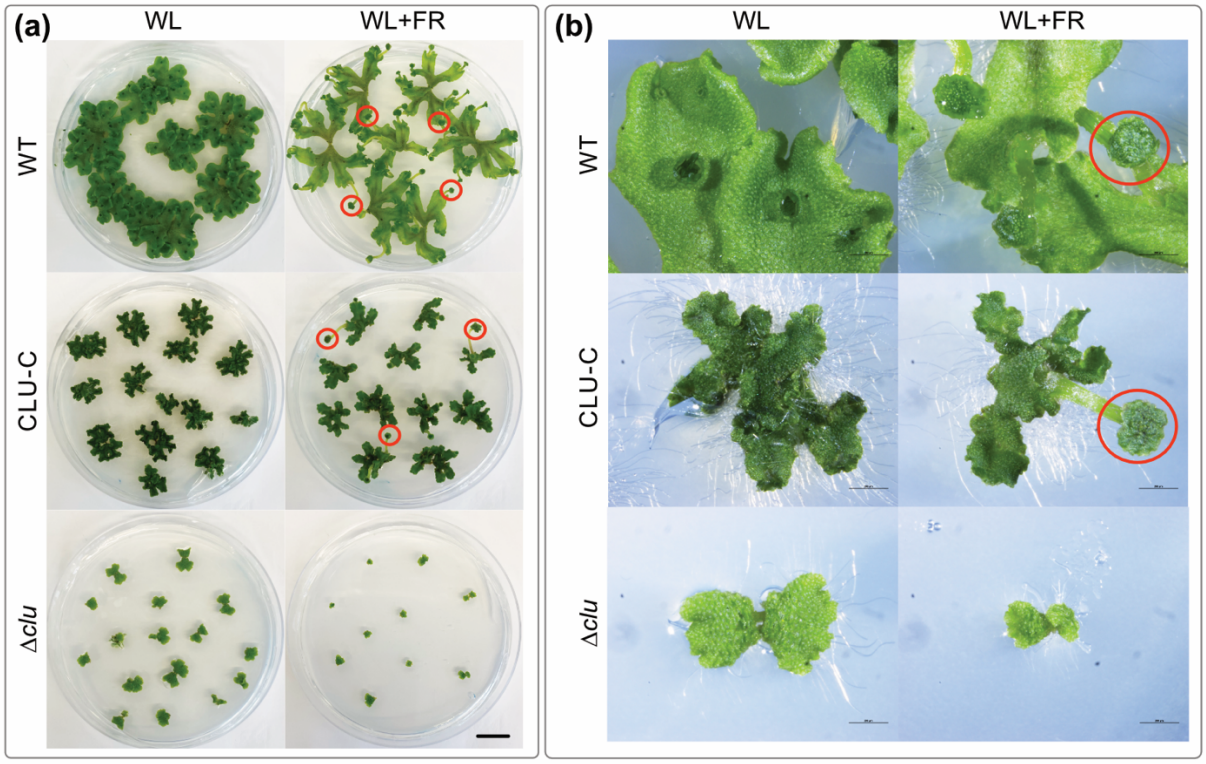

Fig. 5: Δ*clu* and CLU-C::Citrine plants show growth defects and a delay in the formation of reproductive organ. When grown under far-red (FR) light conditions, vegetative-to-reproductive state shift is induced, which involves the formation of gametangiophore structures (red circles). **(a)** 16 days old WT, Δ*clu* and CLU-C::Citrine lines incubated under white light (WL) and WL supplemented with FR light. Scale bar: 1 cm. **(b)** Zoom in pictures of the same plant lines taken with binocular Nikon SMZ18. Scale bar: 0,2 cm

Loss of MpCLU affects photosynthesis performance and pigment profiles

To characterize the photosynthesis performance, we screened the plant lines using pulse amplitude modulation (PAM) imaging. Consistent with a lower level of chlorophyll in the Δ*clu* plants, we observed a significant reduction in the maximum quantum efficiency of their PSII photochemistry (F_v/F_m), hinting at a compromised function of PSII (Fig. 6a, S11). The quantum yield of photochemical energy in PSII (PSII operating efficiency; Y(II), the fraction of open PSII reaction centers (qL), and the electron transport rate (ETR) were lower in *clu*, while the capacity for non-photochemical quenching (NPQ) remained comparable to WT (Fig. 6b, S12). After saturating the photosystems with a pulse of 800 µmol photons m^{-2} s^{-1}, and when Y(II) equalled 0, a pulse of 2 µmol photons m^{-2} s^{-1} was applied to measure recovery. Δ*clu* did not recover as fast as WT in terms of Y(II), YNPQ(II) qL, and ETR, hinting again at a compromised PSII (Fig. 6b, S13). In the complementation lines, MpCLU^{spl22} and MpCLU^{22}, the values

were restored close to WT levels, both under normal and saturating conditions (Fig. 6b, S11-13). In line with photosynthetic performance and pale thalli, Δ*clu* plants showed a significant decline in key pigments such as chlorophyll a, chlorophyll b, lutein, neoxanthin, violaxanthin, and beta-carotene (Fig. 6c). Both proteoforms increased pigment levels to a varying extent, with chlorophyll a, chlorophyll b and neoxanthin levels being fully restored only by MpCLU^{spl22} (Fig. 6c). Altogether, these results indicate that the loss of MpCLU compromises both PSII activity and pigment accumulation, resulting in impaired photosynthetic performance. The complementation of Δ*clu* suggests a stronger contribution of MpCLU^{spl22} in sustaining pigment composition, although both proteoforms seem to restore photosynthetic function to a similar degree.

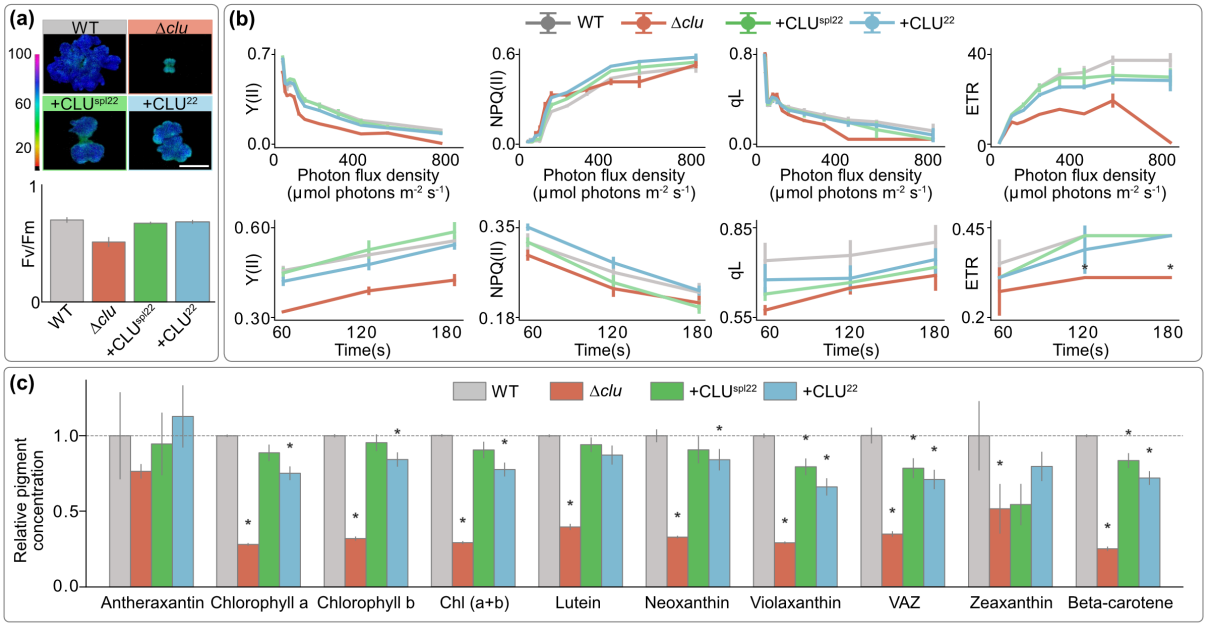

Fig. 6: Photosynthesis and pigment concentration changes in Δclu and complementation lines. (a) Representative images and F_v/F_m values of WT, Δ*clu*, Δ*clu* + CLU^{spl22} and Δ*clu* + CLU^{22}. Scale bar: 1cm. **(b)** Quantification of fluorescence parameters under increasing photon flux density (top): Y(II) as PSII yield, Y(NPQ) indicating regulated heat loss, qL as the fraction of open PSII reaction centres, and electron transport rates (ETR) of plants identical to those listed in a). The same parameters measured with a pulse of 2 µmol photons m^{-2} s^{-1} after PSII is saturated by a pulse of 800 µmol photons m^{-2} s^{-1} and when Y(II)=0 (bottom). **(c)** Fold changes in pigment concentrations relative to the WT. Asterisks indicate significative difference compared to the wild-type (p-value>0.05).

Discussion

Eukaryotic intracellular complexity origin is linked to accommodating an endosymbiont that evolved into mitochondria (Raval et al., 2024; Richards et al., 2024). Critical in this transition, which involved passing over the control over fission from endosymbiont to host, was maintaining an appropriate organelle-to-cell volume ratio. CLU proteins originated under these new constraints and likely supported the early integration of the endosymbiont. Conserved across all eukaryotic supergroups, CLU proteins are an integral part of the machinery ensuring mitochondrial homeostasis. Later, with the endosymbiotic origin of plastids, the first alga faced a similar challenge. The plastid-specific CLU^{pl} family, however, evolved through gene duplication from a CLU^{mt} not before the origin of streptophyte algae and during the transition from a single to multiple plastids per cell (Raval et al., 2024). This evolutionary adaptation links the protein family's function once more to the mechanisms that regulate the cellular volume that is occupied by a compartment of endosymbiotic origin and begs to answer how paralogues (e.g., FMT versus REC in *Arabidopsis*) can distinguish between mitochondria and chloroplast.

The divergence in domain architecture between CLU^{mt} and CLU^{pl} is key to understanding how CLU proteins evolved organelle-specific functions. CLU orthologs contain five predicted domains that offer insights into their specialization. At the N-terminus, the CLU-N domain mediates self-interaction (Ayabe et al., 2021), while the GSK3B interacting protein domain (GSKIP) – more prevalent in CLU^{mt} than CLU^{pl} – is part of an A-kinase anchoring protein complex that binds GSK3β, a kinase involved in microtubule dynamics, cell-cycle progression, metabolism, and transcription factors (N. S. Wu et al., 2022). The function of the CLU-D domain remains uncharacterized, while CLU-C is a domain through which the *Arabidopsis* CLU^{mt} homolog FMT interacts with translation-related proteins such as eIFiso4G1, which is known to increase the translation of chloroplast proteins (Ayabe et al., 2021; Lellis et al., 2019). At the C-terminus, the tetratricopeptide repeats (TPR) domain appears to be crucial for CLU functions, as the deletion of either the TPR domain or CLU-C prevents CLU^{mt} from rescuing the loss-of-function phenotype in *Drosophila*.

The TPR domain of CLU^{mt} is also responsible for mRNA interactions in *Drosophila* and humans and cooperates with the glutamyl-tRNA synthetase OVA9 in *Arabidopsis* (Ayabe et al., 2021; Sen and Cox, 2016). Acetylation of two lysine residues in the plant in proximity to this domain is essential for CLU^{mt} function, as mutating either site prevents molecular complementation (El Zawily et al., 2014). We speculate that this is associated with the need for a functional motif this region represents for outer mitochondrial membrane binding, which at the same time acts as a switch, because lysine acetylation can regulate the binding of peripheral proteins to membranes by masking the positively charges residues that otherwise interact with the negatively charged bilayer (Okada et al., 2021). In *Marchantia*, two lysine residues are only present in MpCLU^{22}, the very variant we find associated with mitochondria. Notably, our phylogenetic analysis of CLU protein clusters and protein domains identify the organization of TPR motifs in the C-terminus to differ between the CLU^{pl} and CLU^{mt} isoforms across species (Fig. 2; S4). This structural variation between CLU^{pl} and CLU^{mt} is also evident in the Mp*CLU* splicing variants. This variation contributes to their functional divergence, likely by either providing an outer mitochondrial membrane binding region or not.

Loss of CLU^{mt} homologs in human, yeast, *Drosophila* and *Arabidopsis* lead to the clustering of mitochondria (Cox and Spradling, 2009; Gao et al., 2014), while the loss of CLU^{pl} homologs leads to an increase in the number of chloroplasts in *Arabidopsis* that, however, occupy less cellular volume in sum (Larkin et al., 2016). The knock-out of the single CLU homolog in *Marchantia* combines effects on mitochondria and chloroplasts, underscoring the general dual-function of the protein in the liverwort. In contrast to what was described for the angiosperm, however, the loss of Mp*CLU* leads to fewer and larger chloroplasts in the bryophyte. Complementation with MpCLU^{spl22} rescues the plastid phenotype but does not mitigate the clustering of mitochondria, while the expression of MpCLU^{22} reduces mitochondrial clustering without restoring the chloroplast phenotype. This is further evidence for a splicing-dependent, functional separation of the two MpCLU proteoforms through a simple change in the C-terminus associated with the TPR and an associated, acetylatable region (Fig. 2a).

While bryophyte genomes in sum encode a larger gene family repertoire than vascular plants (Dong et al., 2025), many genes that are present in multiple copies (paralogs) in the latter are encoded by a single copy in bryophytes; the Mp*CLU* gene of *Marchantia* being one example. Alternative splicing of a single gene can lead to proteins with different functions. The *Arabidopsis* gene *SR45* produces two variants with distinct developmental outputs on the basis of a single exon encoding seven amino acids: the isoform with the seven amino acids controls petal formation, the one lacking it root growth (Zhang and Mount, 2009). In *Marchantia*, the alternative splicing of Mp*SYP7B* generates isoforms that either carry a transmembrane domain or not (Kanazawa et al., 2016). Mp*CLU* offers an example for how to compensate for the evolutionary reduction to a single *CLU* gene, while still needing to serve two organelles of endosymbiotic origin. Alternative splicing of Mp*CLU* was selected for as a solution in

Marchantia and it uncovers the critical region of CLU homologs to focus on with respect to organelle specificity.

It remains uncertain how the CLU protein family measures and or communicates organelle volume and distribution throughout the cell, but the CLU^{pl} homolog REC of *Arabidopsis* has been observed to localise to the nucleus (Larkin et al., 2016). Full length MpCLU^{spl22} localizes to the cytosol and is distributed evenly, consistent with previously reported CLU^{mt} homolog localization (Cox and Spradling, 2009; El Zawily et al., 2014; Kumar et al., 2002), whereas the full-length MpCLU^{22} displayed a punctuated cytosolic distribution, frequently associated with mitochondria. Hence, the exon-dependent difference in the ability to rescue either the mitochondrial or chloroplast phenotype is corroborated by an exon-dependent difference in localization. Considering that also the N-terminal domains (CLU-N and CLU-N + GSKIP), as well as the C-terminus domain including TPR, localize to the cytosol, leaves us only with the CLU-C domain conferring a nuclear localisation, while simultaneously inducing a severe phenotype (Fig. 2). So, while the TPR motif is responsible for organelle specificity, the CLU-C domain appears important for mediating a shuttling of the protein to the nucleus and altering gene expression.

Δ*clu* plants show a severely retarded growth (Fig. 4) and the transcriptome data suggest this is associated with mitochondrial stress, as several mitochondrial stress-responsive genes are upregulated (Fig. S14), which matches previous observations for *Arabidopsis fmt* mutants (El Zawily et al., 2014). In *Drosophila*, the knock-out of Dm*CLU* led to the downregulation of genes for ROS detoxification, DNA repair and apoptosis regulators, while a set of metabolic genes was found to be upregulated(Cox and Spradling, 2009). In humans, CLUH is required to support mitochondrial respiration, amino acid catabolism and β-oxidation (Schatton et al., 2017). Moreover, more than 90% of CLUH-bound mRNAs encode proteins involved in central mitochondrial pathways, including oxidative phosphorylation, citric acid and fatty acid oxidation (Gao et al., 2014). Notably, while many of these targets show reduced protein levels in CLUH knock-outs, their transcript abundance remains unchanged, indicating CLU can also act post-transcriptionally. This is supported by evidence of CLU and its homologs associating with ribosomes at the outer mitochondrial membrane and binding to mitochondrial mRNAs (Gao et al., 2014; Sen and Cox, 2016). In *Marchantia*, the TCA cycle enzyme Mp*OGDH* (Mp4g05670; an ortholog of α-ketoglutarate dehydrogenase) is significantly downregulated in Δ*clu* on the one hand, hinting at a disrupted mitochondrial metabolism, while Mp*AOX1* (Mp6g09630; a canonical marker for mitochondrial damage) is significantly upregulated on the other in CLU-C::Citrine lines (Fig. S14). This speaks for mitochondrial stress in both Δ*clu* and CLU-C::Citrine lines.

The growth deficit of Δ*clu* plants is furthermore caused by a substantial reduction in their photosynthetic performance. Their F_v/F_m is reduced and PSII saturates at lower light intensity compared to WT. Elevated YNPQ(II) indicates that excess excitation energy is preferentially dissipated as heat rather than used for photochemistry. The drop in qL reflects a higher proportion of closed PSII centres, and the electron transport rate (ETR) is significantly impaired. The chloroplasts seem to respond with a higher level of photoprotective mechanisms. In line with the photosynthetic phenotype, total chlorophyll content (chlorophyll a + b) and carotenoid levels are reduced relative to WT (Fig. 6). Transcriptomic analyses showed that Mp*WRKY7* (Mp3g17660), a transcription factor that belongs to the WRKY family, which has been shown in plants to regulate carotenoid biosynthesis genes (Diao et al., 2023), is downregulated in Δ*clu*, but significantly upregulated in the CLU-C::Citrine mutants. That is in line with the dark-green coloured thalli of the CLU-C::Citrine plants (Fig. 2c), which accumulate double the amount of chlorophyll and more carotenoids. The changes in pigment profiles, however, do not translate into a higher photosynthetic efficiency despite the downregulation of early light-induced proteins (ELIP) genes involved in PSII photoprotection.

In line with the pale-looking thalli of Δ*clu*, the marked reduction in chlorophyll and carotenoids reflects a compromised photosynthetic apparatus. Chlorophyll a and b are essential for photon capture and PSII function, while carotenoids play structural and photoprotective roles within PSI/PSII complexes (Wang et al., 2004). Carotenoid absence destabilizes pigment–protein assemblies and reduces the energy dissipation capacity, leading to photoinhibition and impaired PSII performance. Complementation with either MpCLU proteoform was sufficient to restore photosynthetic performance, highlighting Mp*CLU*'s essential role in maintaining chloroplast function. However, pigment levels were mostly fully recovered by MpCLU^{spl22}, which efficiently recovers chlorophyll a/b, lutein, neoxanthin and antheraxanthin, whereas MpCLU^{22} achieved only partial restoration, with a stronger recovery of zeaxanthin, a key component of non-photochemical quenching (NPQ). This difference suggests that although both proteoforms support the core photosynthetic machinery, MpCLU^{spl22} may be more effective in coordinating pigment biosynthesis or stability, while MpCLU^{22} may regulate stress-responsive pathways, pointing toward a functional divergence between the two isoforms or a differential contribution. These findings point to distinct, yet complementary roles for the two proteoforms in chloroplast function and photoprotection.

Complementation of Δ*clu* with MpCLU^{spl22} or MpCLU^{22} partially restores thallus area and biomass, indicating that both isoforms can recover key physiological functions. In a WT background, neither MpCLU^{spl22}::Citrine, MpCLU^{22}::Citrine, nor N-terminal domains fused to Citrine, produce obvious phenotypes, while the expression of CLU-C::Citrine causes semi-dwarfism and a dark-green appearance. These results highlight the critical contribution of the C-terminal region of MpCLU – which also harbours the alternatively spliced exon – to defining CLU function in *Marchantia*, both structurally and physiologically.

In summary, our findings demonstrate that in *Marchantia* a single *CLU* gene participates in the orchestration of both mitochondrial and plastid homeostasis through the alternative splicing of exon 22 – a strategy adopted to maintain regulatory complexity, following bryophyte genome reformatting. We identify changes in the C-terminal region of CLU proteins to be responsible for mediating mitochondrial versus plastid function after gene duplication of a mitochondrial CLU protein in a streptophyte algal ancestor of land plants. In particular the TPR motif is of importance and in CLU^{mt} proteins is likely involved in binding the outer mitochondrial membrane, if not acetylated. CLU proteins are a critical and conserved component of eukaryotic biology and their C-terminal region can now serve as a prime target for future studies to uncover the molecular details of how the protein family exactly contributes to the regulation of mitochondrial and chloroplast distribution and the upkeep of a functional organelle to cell volume ratio.

Materials and methods

Comparative genomics

We traced evolutionary history of organelle distribution control protein using a database of 157 Archaeaplastidal and 10 outgroup eukaryotic genomes (species names and taxonomy summarized in Table S1A). The whole proteome models were clustered using OrthoFinder version 2.5.4 (Emms and Kelly, 2019). The resulting protein clusters were annotated based on the presence of previously characterized proteins involved in organelle volume distribution (Larkin, 2022). Homologues identified as CLU^{mt} and CLU^{pl} (based on the presence of *Arabidopsis* RECs and FRIENDLY in the same cluster) were further analysed for their domain architecture using InterProScan (Larkin, 2022; Paysan-Lafosse et al., 2022) and to predict their proteins structure using AlphaFold (Jumper et al., 2021). The protein cluster network was generated by visualizing BLAST (Buchfink et al., 2014) outputs in Cytoscape.

Plant growth conditions

Marchantia polymorpha (Tak-1 ecotype) was cultivated on half-strength Gamborg´s B5 medium (GVA) containing 1% agar under continuous full light spectrum (450-700nm) 70 µmol m^{-2} s^{-1} at 22°C. Reproductive state was induced by cultivating *Marchantia* with the same light conditions supplemented with far-red light (700-750nm) 40 µmol m^{-2} s^{-1} at 22°C.

Cloning and mutant plants generation

MpCLU^{spl22} (Mp6g08800.1, alias Mapoly0060s0041), MpCLU^{22} (Mp6g08800.2, alias Mapoly0060s0041), and individual domains were amplified from cDNA and cloned into the entry vector pDONR221 (Invitrogen) by Gateway BP reactions set as per manufacturer´s protocol. For localization studies, CLU-N, CLU-N+GSKIP and CLU-C were cloned into the N-terminal side of Citrine on pMpGWB105, and MpCLU^{spl22}, MpCLU^{22} and C-terminal constructs were cloned into the C-terminal side of mCitrine on pMpGWB106 via Gateway LR reactions following manufacturer's protocol. For loss-of-function analyses, CRISPR/Cas9-based genome editing of Mp*CLU* was performed by targeting the first exon of MpCLU. The oligonucleotides containing the target sequences were synthesized and cloned into pMpGE_En03 (Sugano et al., 2018). Generated entry clones were recombined into the expression vector pMpGE010 by Gateway LR Clonase (Thermo Fisher) as per manufacturer's instruction. For complementation of Δclu, the CDS of Mp*CLU*^{spl22} and Mp*CLU*^{22} were cloned into pDONR221 (Invitrogen) and recombined into pMpGWB301 using Gateway LR Clonase (Thermo Fisher).

All expression vectors were transformed into *Agrobacterium tumefaciens* (GV301 without pSoup) by electroporation (Bio-Rad GenePulser Xcell, 1.44 kV). Subsequent plant transformations were carried out as previously described (Raval et al., 2025). The resulting transformants were grown and selected on half-strength Gamborg's B5 media containing 1% phyto agar supplemented with Hygromycin (10 µg/mL) and Cefotaxime (100 µg/mL) for localization and loss-of-function constructs, and 0.5 µM chlorsulfuron to screen complementation constructs. Gemmae from multiple explants were taken forward to the next generation and grown until they produced gemmae, which were further screened. To genotype Marchantia plant lines, 100 mg of thalli from individual plants were used to extract gDNA that was used as a template for polymerase chain reactions.

Microscopy samples preparation

Gemmae from expression-positive plant lines were grown for 24h and placed in 30 µL of water on a slide and covered with a coverslip. Protoplasts were prepared as previously described (Raval et al., 2025). *Marchantia* 1day-old thalli and protoplasts were stained with 500 nM MitoTracker™ CMXRos following manufacturer's instructions. The protoplast or cell suspension were incubated with 500 nM dye for 20 min at room temperature (RT), washed three times by centrifuging the cells at 2,000g and protoplasts at 100g for 5 min to visualize mitochondria.

Fluorescence imaging analysis

Analyses of Citrine, chlorophyll fluorescence and mitochondria were performed according to our previous studies (Raval et al., 2025). Briefly, Nikon Eclipse Ti Imaging platform and confocal laser scanning microscopy (SP8X system, Leica Microsystems, Wetzlar, Germany) were used with the settings previously described (Raval et al., 2025). Autofluorescence from chloroplasts was filtered out by the time-gated method (Kodama, 2016). All localization analyses and microscopy images processing were conducted in ImageJ (Fiji) with the BIOP JACoP plugin (auto thresholds).

Cell quantification and analyses

Chloroplasts and mitochondria from gemmae were traced and measured to analyse number and area using Analyse particles plug-in in ImageJ (1.54f), as well as cell area. Mitochondrial clustering was calculated as the sum of all the areas of mitochondria that had no physical separation between them. Chloroplast coverage was calculated by dividing the total chloroplast area of a cell by the total area of that cell.

Pigments content analysis

For pigment quantification, 50 mg of 14 days old gemmalings were used with three biological replicates per genotype. Tissue was grinded with 1mL acetone and 0.013g magnesium sulfate heptahydrate with a pestle till the sample is consistent. The mixture was filtered out with miracloth paper and stood for 15 min. Samples were centrifuged at 2000 x g speed and the supernatant stood for 30 min at 4°C and stored at -20°C until analysis. The pigment extracts were filtered (0.2 µm pore size) and then used for reversed-phase HPLC as previously described (Farber et al., n.d.).

Measurement of chlorophyll fluorescence

An IMAGING-PAM (M-Series; Walz) was used to assess the photosynthetic parameters in PSII. Pulse amplitude-modulated measuring light (<1 µmol m^{-2} s^{-1}) was applied to determine minimum fluorescence (F_o), and a subsequent saturating pulse of 3000 µmol m^{-2} s^{-1} was used to evaluate maximum fluorescence (F_m and F_m'), and F' is the fluorescence emission. Photosynthetic parameters were calculated using the following formulas: $F_v/F_m = (F_m-F_o)/F_m$', $Y(II)= (F_m' – F')/F_m'$, $NPQ = (F_m – F_m')/F_m'$, and $qP = (F_m' – F')/ (F_m' – F_o)$. During analysis with Imaging-PAM, pulse-modulated excitation and saturation pulses were achieved with a blue light-emitting diode lamp with a peak emission of 450 nm. Images of the photosynthetic parameters were displayed with the help of a false-color code ranging from black (0) to red, yellow, green, blue, and pink (100).

RNA extraction, qPCR and sequencing

RNA was extracted from 14 days old gemmalings using the RNeasy Plant Mini kit (Qiagen). 500 ng of DNase-treated RNA was used as a template for preparing cDNA with iScript™ cDNA Synthesis kit (Bio-Rad) following manufacturer´s instructions. qPCR was performed using GoTaq® qPCR and RT-qPCR Systems kit (Promega). Reaction conditions comprised initial denaturation at 95°C for 5 min followed by 40 cycles of 95°C for 15 seconds (denaturation) and 60°C for 1 minute (annealing, extension and fluorescence reading).

For RNA-sequencing, three biological replicates were prepared for each genotype and mRNA isolated via their poly(A) tail. RNA integrity and concentration were assessed using a NanoDrop spectrophotometer. Libraries were prepared by Eurofins Genomics (Ebersberg, Germany). Sequencing was performed on an Illumina NovaSeq 6000 platform, generating paired-end reads (2 × 150 bp)**,** with an average of ~30 million read pairs per sample. Sequencing data was quality checked and analyzed as described previously (Frangedakis et al., 2024). Briefly, high quality reads were retained using FASTQC and TrimGalore, aligned to *Marchantia polymorpha* genome (v.7.1) using Kallisto (Bowman et al., 2017; Bray et al., 2016) and DEG were obtained through DESeq2 (Love et al., 2014).

Data availability

Supplementary figures and tables are available with this submission. Transcriptome data are available in the NCBI Sequence Read Archive: PRJNA1435946. Supplementary data and figure source data are available on Zenodo (10.5281/zenodo.18985279)

Author contributions

MLQ: conceptualization, supervision; experimental design, investigation, data curation, formal analysis, validation and visualization, writing original draft, review and editing. PKR: conceptualization, supervision, experimental design, formal analysis, visualization, writing original draft, review and editing. SBG: conceptualization; project administration; supervision; experimental design; funding and resource acquisition; data visualization; writing original draft, review and editing.

Funding

We thank the HHU Düsseldorf for support via their SFF program.

Acknowledgements

We acknowledge support from the high-performance computing cluster (HILBERT) and Center for Advanced Imaging (CAi) at the Heinrich Heine University Düsseldorf and thank Michael Knopp, Michelle Kipp, Lennart Schwarz, Sina Kruse, Daniel Wasim Djamriani, and Margarete Stracke for their help. We thank Nora Gutsche and Sabine Zachgo of the University of Osnabrück, and Hirofumi Nakagami and Katharina Kramer of the MPI Cologne for their support with setting up *Marchantia*. We thank Peter Jahns (HHU Düsseldorf) for his help with pigment isolation and photosynthesis performance analysis. MLQ and PKR are grateful to William F. Martin (HHU Düsseldorf) for financial support.

References

Ayabe H, Kawai N, Shibamura M, Fukao Y, Fujimoto M, Tsutsumi N, Arimura S ichi. 2021. FMT, a protein that affects mitochondrial distribution, interacts with translation-related proteins in Arabidopsis thaliana. Plant Cell Reports **40**:327–337. DOI: https://doi.org/10.1007/s00299-020-02634-9, PMID: 33385240

Bowman JL, Kohchi T, Yamato KT, Jenkins J, Shu S, Ishizaki K, Yamaoka S, Nishihama R, Nakamura Y, Berger F, Adam C, Aki SS, Althoff F, Araki T, Arteaga-Vazquez MA, Balasubrmanian S, Barry K, Bauer D, Boehm CR, Briginshaw L, Caballero-Perez J, Catarino B, Chen F, Chiyoda S, Chovatia M, Davies KM, Delmans M, Demura T, Dierschke T, Dolan L, Dorantes-Acosta AE, Eklund DM, Florent SN, Flores-Sandoval E, Fujiyama A, Fukuzawa H, Galik B, Grimanelli D, Grimwood J, Grossniklaus U, Hamada T, Haseloff J, Hetherington AJ, Higo A, Hirakawa Y, Hundley HN, Ikeda Y, Inoue K, Inoue S ichiro, Ishida S, Jia Q, Kakita M, Kanazawa T, Kawai Y, Kawashima T, Kennedy M, Kinose K, Kinoshita T, Kohara Y, Koide E, Komatsu K, Kopischke S, Kubo M, Kyozuka J, Lagercrantz U, Lin SS, Lindquist E, Lipzen AM, Lu CW, De Luna E, Martienssen RA, Minamino N, Mizutani Masaharu, Mizutani Miya, Mochizuki N, Monte I, Mosher R, Nagasaki H, Nakagami H, Naramoto S, Nishitani K, Ohtani M, Okamoto T, Okumura M, Phillips J, Pollak B, Reinders A, Rövekamp M, Sano R, Sawa S, Schmid MW, Shirakawa M, Solano R, Spunde A, Suetsugu N, Sugano S, Sugiyama A, Sun R, Suzuki Y, Takenaka M, Takezawa D, Tomogane H, Tsuzuki M, Ueda T, Umeda M, Ward JM, Watanabe Y, Yazaki K, Yokoyama R, Yoshitake Y, Yotsui I, Zachgo S, Schmutz J. 2017. Insights into Land Plant Evolution Garnered from the Marchantia polymorpha Genome. Cell **171**:287-304.e15. DOI: https://doi.org/10.1016/j.cell.2017.09.030, PMID: 28985561

Bray NL, Pimentel H, Melsted P, Pachter L. 2016. Near-optimal probabilistic RNA-seq quantification. Nature Biotechnology **34**:525–527. DOI: https://doi.org/10.1038/nbt.3519, PMID: 27043002

526 Buchfink B, Xie C, Huson DH. 2014. Fast and sensitive protein alignment using DIAMOND. *Nature*
527 *Methods*. DOI: https://doi.org/10.1038/nmeth.3176, PMID: 25402007

528 Chan YHM, Marshall WF. 2010. Scaling properties of cell and organelle size. *Organogenesis*. DOI:
529 https://doi.org/10.4161/org.6.2.11464, PMID: 20885855

530 Chou HY, Howng SL, Cheng TS, Hsiao YL, Lieu AS, Loh JK, Hwang SL, Lin CC, Hsu CM, Wang
531 C, Lee CI, Lu PJ, Chou CK, Huang CY, Hong YR. 2006. GSKIP is homologous to the axin
532 GSK3β interaction domain and functions as a negative regulator of GSK3β. Biochemistry
533 **45**:11379–11389. DOI: https://doi.org/10.1021/bi061147r, PMID: 16981698

534 Cox RT, Spradling AC. 2009. Clueless, a conserved Drosophila gene required for mitochondrial
535 subcellular localization, interacts genetically with parkin. DMM Disease Models and
536 Mechanisms **2**:490–499. DOI: https://doi.org/10.1242/dmm.002378, PMID: 19638420

537 Diao Q, Tian S, Cao Y, Yao D, Fan H, Zhang Y. 2023. Transcriptome analysis reveals association of
538 carotenoid metabolism pathway with fruit color in melon. Scientific Reports **13**. DOI:
539 https://doi.org/10.1038/s41598-023-31432-y, PMID: 36973323

540 Dong S, Wang S, Li L, Yu J, Zhang Y, Xue JY, Chen Hengchi, Ma J, Zeng Y, Cai Y, Huang W, Zhou
541 X, Wu J, Li J, Yao Y, Hu R, Zhao T, Villarreal A JC, Dirick L, Liu L, Ignatov M, Jin M, Ruan J,
542 He Y, Wang H, Xu B, Rozzi R, Wegrzyn J, Stevenson DW, Renzaglia KS, Chen Hongfeng,
543 Zhang L, Zhang S, Mackenzie R, Moreno JE, Melkonian M, Wei T, Gu Y, Xu X, Rensing SA,
544 Huang J, Long M, Goffinet B, Bowman JL, Van de Peer Y, Liu H, Liu Y. 2025. Bryophytes hold
545 a larger gene family space than vascular plants. Nature Genetics **57**:2562–2569. DOI:
546 https://doi.org/10.1038/s41588-025-02325-9, PMID: 40983756

547 El Zawily AM, Schwarzländer M, Finkemeier I, Johnston IG, Benamar A, Cao Y, Gissot C, Meyer
548 AJ, Wilson K, Datla R, Macherel D, Jones NS, Logan DC. 2014. FRIENDLY regulates
549 mitochondrial distribution, fusion, and quality control in Arabidopsis. Plant Physiology **166**:808–
550 828. DOI: https://doi.org/10.1104/pp.114.243824, PMID: 25165398

551 Emms DM, Kelly S. 2019. OrthoFinder: Phylogenetic orthology inference for comparative genomics.
552 Genome Biology **20**:1–14. DOI: https://doi.org/10.1186/s13059-019-1832-y, PMID: 31727128

553 Farber A, Young AJ, Ruban A V, Horton P, Jahns P. n.d. Dynamics of Xanthophyll-Cycle Activity in
554 Different Antenna Subcomplexes in the Photosynthetic Membranes of Higher Plants' The
555 Relationship between Zeaxanthin Conversion and Nonphotochemical Fluorescence Quenching.
556 *Plant Physiol*.

557 Fields SD, Conrad MN, Clarke M. 1998. The S. cerevisiae CLU1 and D. discoideum cluA genes are
558 functional homologues that influence mitochondrial morphology and distribution. J Cell Sci
559 **12**:1727–27. DOI: https://doi.org/10.1242/jcs.111.12.1717, PMID: 9601101

560 Frangedakis E, Yelina NE, Billakurthi K, Hua L, Schreier T, Dickinson PJ, Tomaselli M, Haseloff J,
561 Hibberd JM. 2024. MYB-related transcription factors control chloroplast biogenesis. Cell. DOI:
562 https://doi.org/10.1016/j.cell.2024.06.039

563 Gao J, Schatton D, Martinelli P, Hansen H, Pla-Martin D, Barth E, Becker C, Altmueller J, Frommolt
564 P, Sardiello M, Rugarli EI. 2014. CLUH regulates mitochondrial biogenesis by binding mRNAs
565 of nuclear-encoded mitochondrial proteins. Journal of Cell Biology **207**:213–223. DOI:
566 https://doi.org/10.1083/jcb.201403129, PMID: 25349259

Hu Q, Zhang H, Song Y, Song L, Zhu L, Kuang H, Larkin RM. 2024. REDUCED CHLOROPLAST COVERAGE proteins are required for plastid proliferation and carotenoid accumulation in tomato. Plant Physiology. DOI: https://doi.org/10.1093/plphys/kiae275

Jevtić P, Edens LJ, Vuković LD, Levy DL. 2014. Sizing and shaping the nucleus: Mechanisms and significance. *Current Opinion in Cell Biology*. DOI: https://doi.org/10.1016/j.ceb.2014.01.003, PMID: 24503411

Jumper J, Evans R, Pritzel A, Green T, Figurnov M, Ronneberger O, Tunyasuvunakool K, Bates R, Žídek A, Potapenko A, Bridgland A, Meyer C, Kohl SAA, Ballard AJ, Cowie A, Romera-Paredes B, Nikolov S, Jain R, Adler J, Back T, Petersen S, Reiman D, Clancy E, Zielinski M, Steinegger M, Pacholska M, Berghammer T, Bodenstein S, Silver D, Vinyals O, Senior AW, Kavukcuoglu K, Kohli P, Hassabis D. 2021. Highly accurate protein structure prediction with AlphaFold. Nature **596**:583–589. DOI: https://doi.org/10.1038/s41586-021-03819-2, PMID: 34265844

Kanazawa T, Era A, Minamino N, Shikano Y, Fujimoto M, Uemura T, Nishihama R, Yamato KT, Ishizaki K, Nishiyama T, Kohchi T, Nakano A, Ueda T. 2016. SNARE molecules in Marchantia polymorpha: Unique and conserved features of the membrane fusion machinery. Plant and Cell Physiology **57**:307–324. DOI: https://doi.org/10.1093/pcp/pcv076, PMID: 26019268

Kodama Y. 2016. Time gating of chloroplast autofluorescence allows clearer fluorescence imaging in planta. PLoS ONE **11**. DOI: https://doi.org/10.1371/journal.pone.0152484, PMID: 27027881

Kumar A, Agarwal S, Heyman JA, Matson S, Heidtman M, Piccirillo S, Umansky L, Drawid A, Jansen R, Liu Y, Cheung KH, Miller P, Gerstein M, Shirleen Roeder G, Snyder M. 2002. Subcellular localization of the yeast proteome. Genes and Development **16**:707–719. DOI: https://doi.org/10.1101/gad.970902, PMID: 11914276

Larkin RM. 2022. Recent progress on mechanisms that allocate cellular space to plastids. *Fundamental Research*. DOI: https://doi.org/10.1016/j.fmre.2022.09.004

Larkin RM, Stefano G, Ruckle ME, Stavoe AK, Sinkler CA, Brandizzi F, Malmstrom CM, Osteryoung KW, Chory J. 2016. REDUCED CHLOROPLAST COVERAGE genes from Arabidopsis thaliana help to establish the size of the chloroplast compartment. Proceedings of the National Academy of Sciences of the United States of America **113**:E1116–E1125. DOI: https://doi.org/10.1073/pnas.1515741113, PMID: 26862170

Lellis AD, Patrick RM, Mayberry LK, Lorence A, Campbell ZC, Roose JL, Frankel LK, Bricker TM, Hellmann HA, Mayberry RW, Zavala AS, Choy GS, Wylie DC, Abdul-Moheeth M, Masood A, Prater AG, Van Hoorn HE, Cole NA, Browning KS. 2019. EIFiso4G augments the synthesis of specific plant proteins involved in normal chloroplast function. Plant Physiology **181**:85–96. DOI: https://doi.org/10.1104/pp.19.00557, PMID: 31308150

Lloyd AC. 2013. The regulation of cell size. 154 **6**:1194–205. DOI: https://doi.org/10.1016/j.cell.2013.08.053, PMID: 24034244

Logan DC, Scott L, Tobin AK. 2003. The genetic control of plant mitochondrial morphology and dynamics. Plant Journal **36**:500–509. DOI: https://doi.org/10.1046/j.1365-313X.2003.01894.x, PMID: 14617080

Loh JK, Lin CC, Yang MC, Chou CH, Chen WS, Hong MC, Cho CL, Hsu CM, Cheng JT, Chou AK, Chang CH, Tseng CN, Wang CH, Lieu AS, Howng SL, Hong YR. 2015. GSKIP- and GSK3-

609 mediated anchoring strengthens cAMP/PKA/Drp1 axis signaling in the regulation of
610 mitochondrial elongation. Biochimica et Biophysica Acta - Molecular Cell Research **1853**:1796–
611 1807. DOI: https://doi.org/10.1016/j.bbamcr.2015.04.013, PMID: 25920809

612 Love MI, Huber W, Anders S. 2014. Moderated estimation of fold change and dispersion for RNA-seq
613 data with DESeq2. Genome Biology **15**. DOI: https://doi.org/10.1186/s13059-014-0550-8,
614 PMID: 25516281

615 Ma J, Liang Z, Zhao J, Wang P, Ma W, Mai KK, Fernandez Andrade JA, Zeng Y, Grujic N, Jiang L,
616 Dagdas Y, Kang BH. 2021. Friendly mediates membrane depolarization-induced mitophagy in
617 Arabidopsis. Current Biology **31**:1931-1944.e4. DOI: https://doi.org/10.1016/j.cub.2021.02.034,
618 PMID: 33711250

619 Okada AK, Teranishi K, Ambroso MR, Isas JM, Vazquez-Sarandeses E, Lee JY, Melo AA, Pandey P,
620 Merken D, Berndt L, Lammers M, Daumke O, Chang K, Haworth IS, Langen R. 2021. Lysine
621 acetylation regulates the interaction between proteins and membranes. Nature Communications
622 **12**. DOI: https://doi.org/10.1038/s41467-021-26657-2, PMID: 34753925

623 Paysan-Lafosse T, Blum M, Chuguransky S, Grego T, Pinto BL, Salazar GA, Bileschi ML, Bork P,
624 Bridge A, Colwell L, Gough J, Haft DH, Letunić I, Marchler-Bauer A, Mi H, Natale DA, Orengo
625 CA, Pandurangan AP, Rivoire C, Sigrist CJA, Sillitoe I, Thanki N, Thomas PD, Tosatto SCE,
626 Wu CH, Bateman A. 2022. InterPro in 2022. Nucleic Acids Research **51**:418–427. DOI:
627 https://doi.org/10.1093/nar/gkac993

628 Raval PK, García CG, Sanchez M-DS, Gould SB. 2025. Evolutionary refinement of mitochondrial and
629 plastid targeting sequences coincides with the late diversification of land plants. Molecular
630 Biology and Evolution. DOI: https://doi.org/10.1093/molbev/msaf240, PMID: 40986664

631 Raval PK, Garg SG, Gould SB. 2022. Endosymbiotic selective pressure at the origin of eukaryotic cell
632 biology. eLife **11**:1–23. DOI: https://doi.org/10.7554/ELIFE.81033, PMID: 36355038

633 Raval PK, MacLeod AI, Gould SB. 2024. A molecular atlas of plastid and mitochondrial proteins
634 reveals organellar remodeling during plant evolutionary transitions from algae to angiosperms.
635 PLoS Biology **22**. DOI: https://doi.org/10.1371/journal.pbio.3002608, PMID: 38713727

636 Richards TA, Eme L, Archibald JM, Leonard G, Coelho SM, de Mendoza A, Dessimoz C, Dolezal P,
637 Fritz-Laylin LK, Gabaldón T, Hampl V, Kops GJPL, Leger MM, Lopez-Garcia P, McInerney
638 JO, Moreira D, Muñoz-Gómez SA, Richter DJ, Ruiz-Trillo I, Santoro AE, Sebé-Pedrós A, Snel
639 B, Stairs CW, Tromer EC, van Hooff JJE, Wickstead B, Williams TA, Roger AJ, Dacks JB,
640 Wideman JG. 2024. Reconstructing the last common ancestor of all eukaryotes. PLoS Biology
641 **22**. DOI: https://doi.org/10.1371/journal.pbio.3002917, PMID: 39585925

642 Schatton D, Pla-Martin D, Marx MC, Hansen H, Mourier A, Nemazanyy I, Pessia A, Zentis P, Corona
643 T, Kondylis V, Barth E, Schauss AC, Velagapudi V, Rugarli EI. 2017. CLUH regulates
644 mitochondrial metabolism by controlling translation and decay of target mRNAs. The Journal of
645 cell biology **216**:675–693. DOI: https://doi.org/10.1083/jcb.201607019, PMID: 28188211

646 Sen A, Cox RT. 2016. Clueless is a conserved ribonucleoprotein that binds the ribosome at the
647 mitochondrial outer membrane. Biology Open **5**:195–203. DOI:
648 https://doi.org/10.1242/bio.015313

649 Sengupta D, Linstedt AD. 2011. Control of organelle size: The Golgi complex. Annual Review of Cell
650 and Developmental Biology **27**:57–77. DOI: https://doi.org/10.1146/annurev-cellbio-100109-
651 104003, PMID: 21639798

652 Stanley LE, Ding B, Sun W, Mou F, Hill C, Chen S, Yuan YW. 2020. A tetratricopeptide repeat
653 protein regulates carotenoid biosynthesis and chromoplast development in monkeyflowers
654 (Mimulus). Plant Cell **32**:1536–1555. DOI: https://doi.org/10.1105/tpc.19.00755, PMID:
655 32132132

656 Sugano SS, Nishihama R, Shirakawa M, Takagi J, Matsuda Y, Ishida S, Shimada T, Hara-Nishimura
657 I, Osakabe K, Kohchi T. 2018. Efficient CRISPR/Cas9-based genome editing and its application
658 to conditional genetic analysis in Marchantia polymorpha. PLoS ONE **13**. DOI:
659 https://doi.org/10.1371/journal.pone.0205117, PMID: 30379827

660 Wang Y, Mao L, Hu X. 2004. Insight into the Structural Role of Carotenoids in the Photosystem I: A
661 Quantum Chemical Analysis.

662 Wu NS, Lin YF, Ma IC, Ko HJ, Hong YR. 2022. Many faces and functions of GSKIP: a
663 temporospatial regulation view. Cellular Signalling **97**. DOI:
664 https://doi.org/10.1016/j.cellsig.2022.110391, PMID: 35728705

665 Wu Y, Pegoraro AF, Weitz DA, Janmey P, Sun SX. 2022. The correlation between cell and nucleus
666 size is explained by an eukaryotic cell growth model. PLoS Computational Biology **18**. DOI:
667 https://doi.org/10.1371/journal.pcbi.1009400, PMID: 35180215

668 Yang H, Sibilla C, Liu R, Yun J, Hay BA, Blackstone C, Chan DC, Harvey RJ, Guo M. 2022.
669 Clueless/CLUH regulates mitochondrial fission by promoting recruitment of Drp1 to
670 mitochondria. Nature Communications **13**. DOI: https://doi.org/10.1038/s41467-022-29071-4,
671 PMID: 35332133

672 Zhang XN, Mount SM. 2009. Two alternatively spliced isoforms of the Arabidopsis SR45 protein
673 have distinct roles during normal plant development. Plant Physiology **150**:1450–1458. DOI:
674 https://doi.org/10.1104/pp.109.138180, PMID: 19403727

675 Zhang Y, Peng Y, Liu J, Yan J, Zhu K, Sun X, Bu X, Wang X, Ahammed GJ, Liu Y, Sun Z, Qi M,
676 Wang F, Li T. 2023. Tetratricopeptide repeat protein SlREC2 positively regulates cold tolerance
677 in tomato. Plant Physiology **192**:648–665. DOI: https://doi.org/10.1093/plphys/kiad085

678 Zhu Q, Hulen D, Liu T, Clarke M. 1997. The cluA mutant of Dictyostelium identifies a novel class of
679 proteins required for dispersion of mitochondria. *Cell Biology Communicated by James A.*
680 *Spudich*.

681